AGU PUBLICATIONS

JGR

Journal of Geophysical Research: Planets

RESEARCH ARTICLE
10.1002/2016JE005041

Key Points:
- Variations in 70 cm radar backscatter across Mare Imbrium provide a unique means with which to map volcanic units
- The radar-derived map of Imbrium provides evidence of stratigraphic relationships between four discrete volcanic units
- The radar map also places important constraints on the interpretation of the Chang'e-3 Lunar Penetrating Radar measurements

Correspondence to:
G. A. Morgan,
morganga@si.edu

Citation:
Morgan, G. A., B. A. Campbell, D. B. Campbell, and B. R. Hawke (2016), Investigating the stratigraphy of Mare Imbrium flow emplacement with Earth-based radar, *J. Geophys. Res. Planets*, *121*, 1498–1513, doi:10.1002/2016JE005041.

Received 24 MAR 2016
Accepted 26 JUL 2016
Accepted article online 30 JUL 2016
Published online 26 AUG 2016

Investigating the stratigraphy of Mare Imbrium flow emplacement with Earth-based radar

G. A. Morgan[1], B. A. Campbell[1], D. B. Campbell[2], and B. R. Hawke[3,4]

[1]Center for Earth and Planetary Studies, Smithsonian Institution, Washington, District Columbia, USA, [2]Department of Astronomy, Cornell University, Ithaca, New York, USA, [3]HIGP, University of Hawai'i at Mānoa, Honolulu, HI, USA, [4]Deceased 24 January 2015

Abstract The lunar maria are the product of extensive basaltic volcanism that flooded widespread portions of the Moon's surface. Constraining mare volcanic history therefore provides a window into the endogenic processes responsible for shaping the Moon. Due to the low magma viscosity and the associated thin nature of lava units, the majority of mare surface structures are masked and subdued by impact regolith. Subtle individual mare flow morphologies, coupled with spatial limitations in the use of crater size distributions to distinguish surface units close in age, restrict our understanding of mare stratigraphy. Earth-based 70 cm wavelength (P band) radar can reveal features beneath the regolith and highlight very subtle changes in the ilmenite content of the flows, providing a unique means to map mare units. Here we map volcanic units in Mare Imbrium using high-resolution (200 m/pixel), Earth-based P band data. Situated within the heat-producing potassium, rare earth element, and phosphorus terrane, Mare Imbrium experienced some of the most long-lived (and recent) lunar volcanism, and its surface exhibits a significant diversity of basaltic chemistry. Our investigation identifies at least four distinct stages of volcanic activity, originating from multiple sources within Imbrium. The most recent of these stages comprises extensive, yet relatively thin volcanic flow units that left remnant kipukas of older mare material distributed across much of the basin. From a future mission perspective, it may be possible to collect samples expressing a wide range in age from small areas of Mare Imbrium. Our map also places important constraints on the interpretation of the Chang'e-3 Lunar Penetrating Radar measurements.

1. Introduction

The 6.5×10^{-6} km^2 of basaltic flows that make up the lunar maria [*Head*, 1975] represent the most fundamental exogenic process to have resurfaced the face of the Moon. Samples collected during the Apollo and Luna missions of the late 1960s–1970s provide a radiometric age range for mare formation of 3.1–4.3 Ga [e.g., *Taylor*, 1982; *Taylor et al*., 1983; *Nyquist and Shih*, 1992; *Nyquist et al*., 2001]. As noted by *Morota et al*. [2011], this range is extended by the lunar meteorite collection, which includes a basaltic sample with a minimum age of 2.7 Ga [*Borg et al*., 2007]. Based on their similar scales, comparisons have been drawn between terrestrial interplate large igneous provinces and the lunar maria [e.g., *Head and Coffin*, 1997]. However, the growing recognition of the >100-fold difference in duration of activity argues that mare formation represents a form of volcanism distinct from that experienced on Earth [*Bryan and Ferrari*, 2013] and may represent a unique volcanic phenomenon within the solar system.

In contrast to the Earth, Venus, and Mars, the majority of individual mare flow morphologies are subdued—due in part to the low eruptive magma viscosity and the associated thin nature of lunar lava—and thus are masked by impact regolith. Reconstructing the volcanic history of the maria is therefore problematic. In order to map the eruptive units that comprise the surface of the mare and investigate the associated stratigraphic relationships, multiple studies have exploited mineralogical variations inferred from ultraviolet-near infrared (UV-NIR) spectral data [*Soderblom et al*., 1977; *Pieters*, 1978; *Hiesinger et al*., 2000, 2003; *Bugiolacchi and Guest*, 2008; *Thiessen et al*., 2014]. This spectral analysis has shown the lunar sample collection to represent only a subset of the full suite of basaltic chemistry present on the Moon's surface [e.g., *Pieters*, 1978]. Correspondingly, age estimates from various techniques have revealed a significantly extended period of mare activity, with the youngest flows having potentially been emplaced 100 Ma [*Braden et al*., 2014] and larger-scale eruptions occurring as recently as ~1.5 Ga [*Hiesinger et al*., 2000; *Morota et al*., 2011; *Fassett and Thomson*, 2014]. The youngest episodes of mare volcanism have been identified within Ocean Procellarum and western Imbrium [*Hiesinger et al*., 2000, 2003]. This region (Figure 1) is situated at the center of the

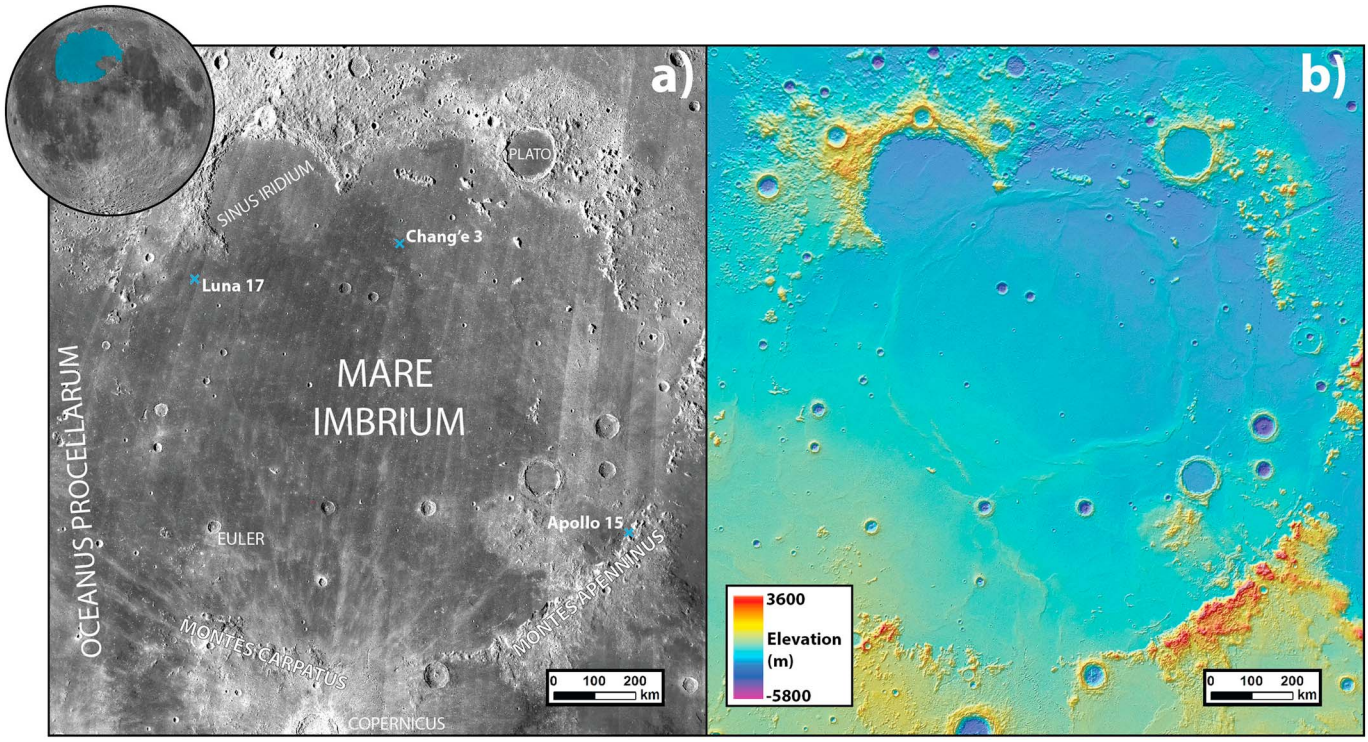

Figure 1. Mare Imbrium. (a) LROC WA camera mosaic highlighting the locations of the three missions to have landed within the basin. (b) LROC WA camera stereo-derived DTM.

potassium, rare earth element, and phosphorus terrain, and the concentration of associated heat-producing elements is presumed responsible for the extended duration of eruptions [*Ziethe et al*., 2009]. Lava flows within Mare Imbrium are particularly unique in that topographically distinct flow fronts are present and easily identifiable in image and topographic data [*Schaber*, 1973] (Figure 2). Through the mapping of these flows and albedo differences, *Schaber* [1973] provided a first-order investigation of the stratigraphy of volcanic units (Figure 3a). However, *Schaber's* [1973] stratigraphy and crater size-frequency distribution (CSFD)-derived age estimates [*Hiesinger et al*., 2000; *Morota et al*., 2011] show contrasting results, which likely result from the level of uncertainty within CSFD age estimates. Further refinement of the nature, age, and stratigraphic relationships of mare emplacement are therefore essential to our continued understanding of the thermal history of the Moon.

Radar studies using Earth-based P band (70 cm wavelength) radar (Figure 4a) provide additional insights into the volcanic structure of the maria [*Campbell et al*., 1997, 2007, 2008, 2009, 2010, 2014]. P band radar signals can probe well beneath the mare regolith surface to provide information on the rocky transition zone situated just above the intact bedrock, which comprises the remains of the most recent basaltic flows. *Campbell et al*. [2014] demonstrated in a study of Mare Serenitatis that P band radar echoes are highly sensitive to the microwave loss properties of the regolith, which are in turn modulated by the ilmenite content of the original lava flows from which the regolith originated. Unlike spectral maps of specific mineral concentrations, such as TiO_2 [*Lucey et al*., 2000] (Figure 5) or maps derived from the absorption properties of multiple mafic assemblages [*Hiesinger et al*., 2000; *Thiessen et al*., 2014] (Figures 3b and 3c), which are only sensitive to the upper few microns of the surface, the penetration depth of the P band signal ($>$10 m) enables the full vertical column of the regolith to be sampled. As a result, the radar echoes are less influenced by contamination from thin surficial deposits, such as rays and ejecta blankets composed of highlands or basaltic material of a different composition to that of the local area. *Campbell et al*. [2014] were able to identify a host of previously unseen volcanic features, including flow unit boundaries and channels interpreted to be the collapsed remnants of plumbing systems similar to those of terrestrial basaltic volcanic fields.

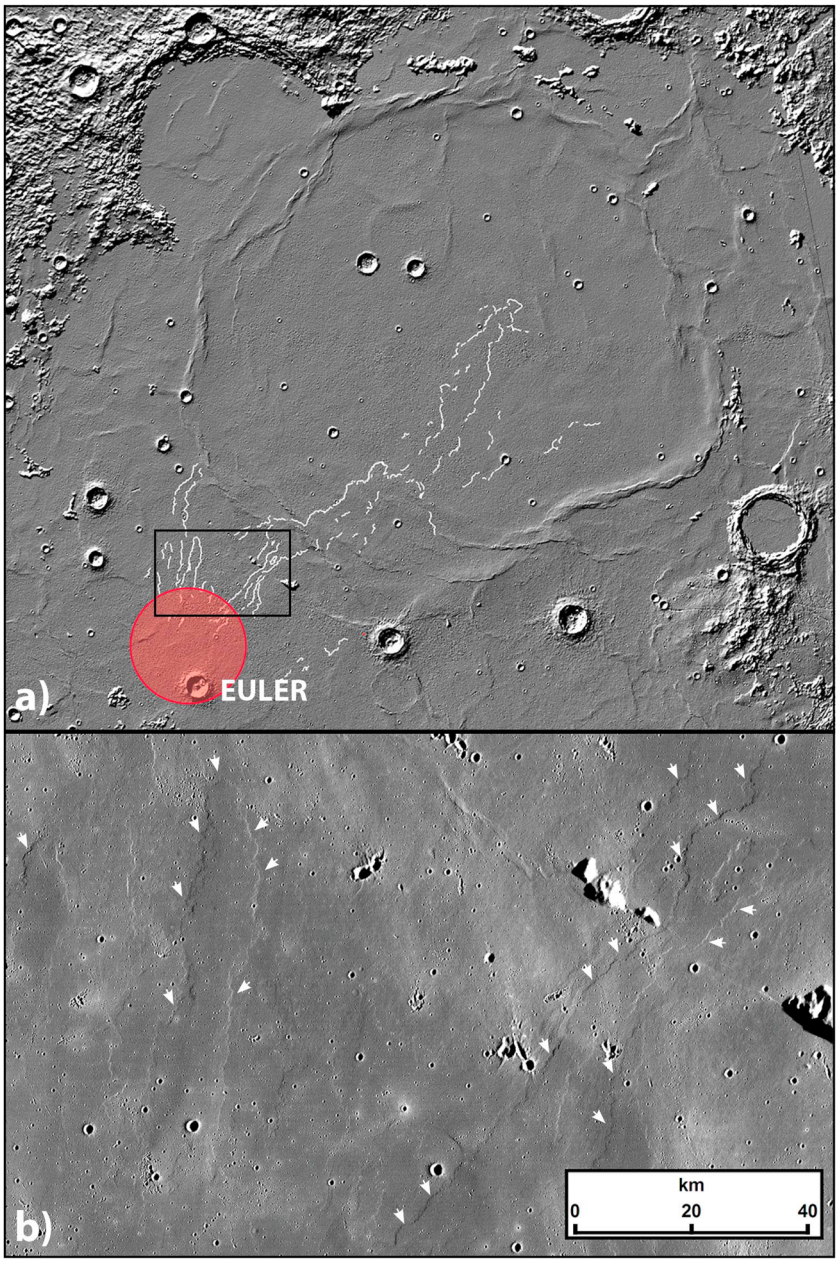

Figure 2. (a) Map of topographically raised flow fronts within Mare Imbrium. The white lines highlight the margins of mare flow fronts, and the red circle denotes their potential source region as proposed by *Schaber* [1973]. (b) The map was produced from observations using the low sun angle LROC WA image mosaic. The white arrows highlight the locations of the flow fronts. Note that the background of Figure 2a is a hillshade image derived from the 100 m LROC WA DTM.

The radar map derived by *Campbell et al*. [2014] permitted unit delineation within Mare Serenitatis to be improved and helped to reconcile inconsistencies between regional stratigraphic relationships [*Weider et al*., 2010] and crater count age dating [*Hiesinger et al*., 2000]. P band radar therefore represents a powerful tool in the determination and refinement of mare unit boundaries. Here we apply the methodology of *Campbell et al*. [2014] to map flow units across Mare Imbrium and to explore the nature and stratigraphy of the extensive volcanism that occurred within the basin. Taking advantage of the presence of topographic flow boundaries (Figure 2) and previous mapping efforts (Figure 3b and 3c), we apply recently acquired, high-resolution P band radar data (Figure 4) to further refine the geologic history of Mare Imbrium. We first analyze the disparities between previous stratigraphic studies, then present, and discuss improvements enabled by the radar mapping.

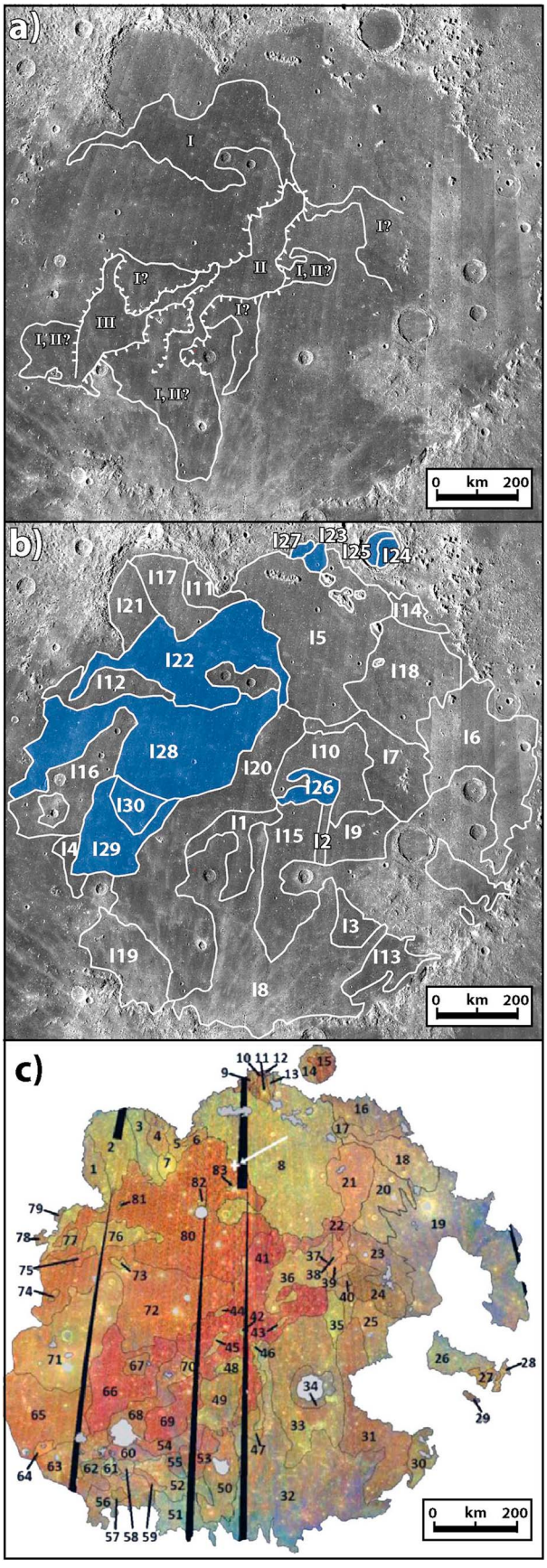

2. Mare Imbrium

Mare Imbrium is over 1100 km in diameter (Figure 1) and represents the largest volcanic deposit to have flooded a lunar impact basin. Determining the thickness of mare deposits is problematic due to uncertainties in the preexisting basin topography, but multiple techniques have been employed to provide constraints. These include computational experiments, which synthetically flood the exposed Archimedes-Apennine bench in southeastern Imbrium to match actual mare surfaces [*Head*, 1982] and studies of the morphometric properties of buried craters [*De Hon*, 1979; *Thomson et al.*, 2009], both of which estimate a thickness of at least 1 km. The Kaguya radar sounder added further support for this minimum estimate, through the identification of multiple subsurface reflectors within central northern Imbrium, the deepest of which was at an apparent depth of 1050 m [*Ono et al.*, 2009]. This value is consistent with subsurface structures identified by the Apollo 17 sounder within Maria Serenitatis and Crisium [*Peeples et al.*, 1978].

The occurrence of topographically definable flow lobes and large-scale surface albedo variations enabled *Schaber* [1973] to map the youngest (Eratosthenian) lava flows within Mare Imbrium from Apollo 15 and 17 orbital image data (Figure 3a). This work identified three different phases of mare emplacement (flows I–III, see Figure 3a), each corresponding to a smaller surface area than the previous. Based on the apparent

Figure 3. Maps of Mare Imbrium. (a) *Schaber* [1973], (b) *Hiesinger et al.* [2000], and (c) *Thiessen et al.* [2014]. Note that the portions of the Hiesinger map [2000] highlighted in blue represent surface units for which *Morota et al.* [2011] also provided age estimates.

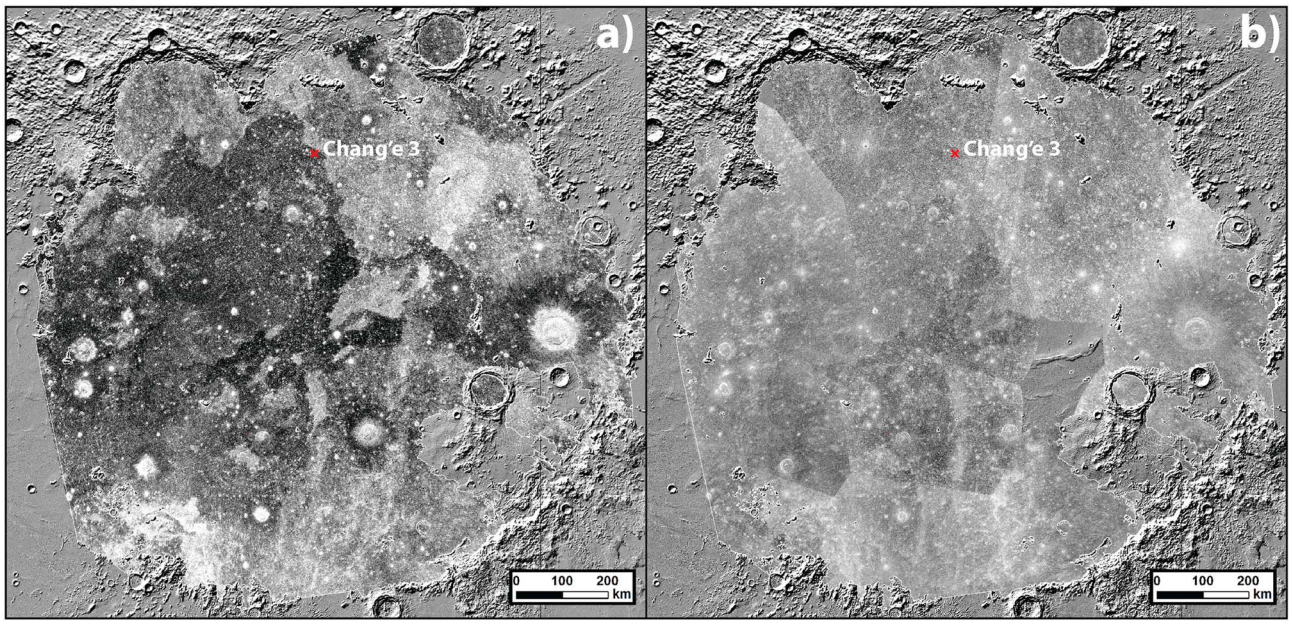

Figure 4. Radar maps of Mare Imbrium. (a) P band SC radar coverage. (b) Mosaic of S band SC coverage. Note both data sets are embedded within a LROC WAC DTM-derived Hillshade image. The highland/mare boundaries were derived from shapefiles provided by the LROC team online at http://lroc.sese.asu.edu/data/LRO-L-LROC-5-RDR-V1.0/LROLRC_2001/EXTRAS/SHAPEFILE/LUNAR_MARE/.

flow direction of the mare units, *Schaber* [1973] proposed that the source region for the flows was close to the 28 km diameter Euler crater (Figures 2a and 3a). UV-IR spectral data provide an additional means to identify regions of homogeneous mafic mineralogy [*Hiesinger et al*., 2000, 2003; *Bugiolacchi and Guest*, 2008; *Thiessen et al*., 2014]. Utilizing Clementine data, *Hiesinger et al*. [2000, 2011] subdivided Mare Imbrium into 30 units (Figure 3b), 7 of which (see Table 1) display strong correlations with the *Schaber* [1973] map (Figure 3a). The recent availability of higher spectral resolution M^3 data has permitted a reclassification of Imbrium into 83 units [*Thiessen et al*., 2014] (Figure 3c).

Three missions have landed on the surface of Mare Imbrium (Figure 1a). Apollo 15, which explored the Hadley rille region along the Montes Apenninus, is the only mission to return Imbrium basalt samples. The Soviet Luna 17 and the recent Chinese Chang'e-3 mission both included rovers and investigated different regions of western Imbrium on the opposite side of the basin to Apollo 15. Both rover missions landed within a region mapped as part of *Schaber's* [1973] flow I unit. The Chang'e-3 rover was the first mission to deploy a radar instrument on the lunar surface (the lunar penetrating radar, LPR), enabling an investigation of the subsurface with a higher range and horizontal spatial resolution than is possible from orbital sounders. The LPR results reveal a complex subsurface structure expressed as multiple reflecting layers down to a depth of over 300 m below the landing site [*Xiao et al*., 2015; *Zhang et al*., 2015]. However, disagreements exist regarding the geologic interpretation of these reflectors. *Xiao et al*. [2015] argue that the youngest flow unit at the landing site (flow I [*Schaber*, 1973) is ~40 m thick and is situated above a paleoregolith layer, suggesting that it is temporally separated from the lower flows. In contrast, *Zhang et al*. [2015] disregard these potential shallower structures in the radar data and propose that a deeper reflector (~195 m) represents the actual base of the flow. The two studies also disagree on the nature of the regolith at the landing site. The occurrence of a nearby 450 m diameter crater led *Xiao et al*. [2015] to suggest that the rover traversed above a several meter thick upper layer of ejecta that overlies a similarly thick layer of mare impact regolith. *Zhang et al*. [2015] estimate a similar thickness for the regolith of ~5 m but argued that the ejecta component is negligible. An analysis by *Fa et al*. [2015] of the high-frequency channel LPR data provides further support for the existence of an ejecta blanket; however, additional studies are clearly required to further constrain the thickness of the basaltic flow units that lie below the surficial regolith/ejecta layers.

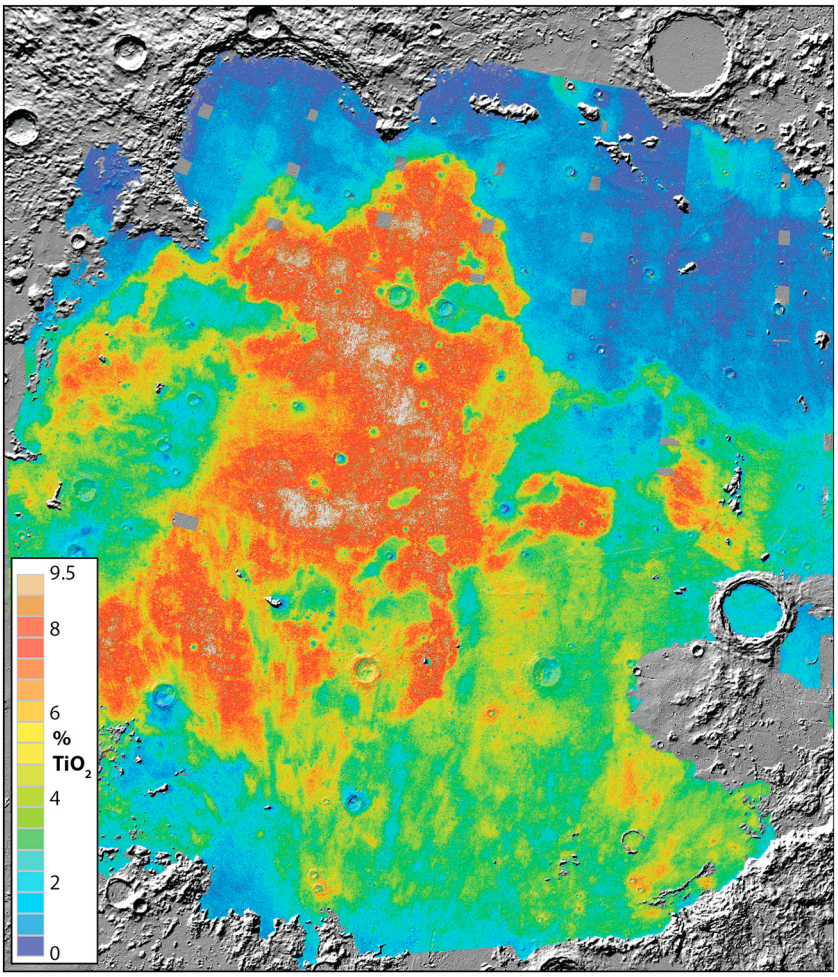

Figure 5. Clementine Map of TiO_2 concentration within Mare Imbrium. The map was generated using *Lucey et al.* [2000] methodology.

3. Limits to Establishing Surface Age Distributions: A Motivation for Radar Mapping

Assuming the UV-IR spectral map units to be representative of distinct eruption episodes, impact crater populations can be used to derive age estimates and constrain mare stratigraphy. Lunar crater production functions and crater chronologies which tie the age of a surface to the abundance of craters larger than a specific size (usually 1 km diameter) per unit area [*Neukum*, 1983; *Neukum et al.*, 2001; *Neukum and Ivanov*, 1994]

Table 1. Comparison Between the Topographically Definable Volcanic Flow Stratigraphy Established by *Schaber* [1973] and CSFD Age Estimates of Equivalent Surface Units

Schaber [1973] Flows (Oldest to Youngest)	*Hiesinger et al.* [2000] Equivalent Units	*Hiesinger et al.* [2000] Ages (Ga)	*Morota et al.* [2011] Ages (Ga)
I	I1	3.57 + 0.07/−0.02	-
	I7	3.47 + 0.05/−0.06	-
	I22	2.96 + 0.13/−0.17	2.29 + 0.09/−0.10
	I30	2.01 + 0.14/−0.14	2.27 + 0.14/−0.16
I, II	I4	3.53 + 0.06/−0.08	2.34 + 0.13/−0.13
	I20	3.01 + 0.12/−0.16	-
	I26	2.70 + 0.17/−0.17	2.29 + 0.11/−0.12
II	I20	3.01 + 0.12/−0.16	-
III	I29	2.26 + 0.16/−0.15	2.15 + 0.07/−0.07

can be applied to CSFD to derive absolute surface ages. This approach has proved a powerful means of assessing the global range of mare surface ages and in determining the youngest volcanic provinces on the Moon [*Hiesinger et al*., 2000, 2011]. Such studies provide a surface age range for Mare Imbrium of 2.01–3.57 Ga [*Hiesinger et al*., 2000].

Error analyses associated with crater count-derived age estimates demonstrate the limitations associated with distinguishing surfaces close in age [*Hiesinger et al*., 2000; *Morota et al*., 2011]. In the case of Mare Imbrium, on average each of the 30 surface units mapped and dated by *Hiesinger et al*. [2000] is chronologically indistinguishable from the age date of 10 of the other 29 units. Establishing stratigraphic relationships between individual units within a lunar mare based on CSFD is therefore problematic. To highlight this, Table 1 compares the *Hiesinger et al*. [2000] crater-derived ages for mare surface units that spatially correspond to the three stratigraphic units mapped by *Schaber* [1973]. The *Schaber* [1973] flow units represent the most recent volcanic activity, but crater-derived ages for the three phases span the full temporal range exhibited over the entire surface of Mare Imbrium [*Hiesinger et al*., 2000], and some units have an estimated age that falls outside of the Eratosthenian age proposed by *Schaber* [1973]. The crater-derived relative ages also do not always agree with the *Schaber* [1973] stratigraphy (Table 1). For example, *Hiesinger et al*. [2000] unit I28, which comprises surfaces embayed by all three of the *Schaber* [1973] flow units (Figure 3), has an age estimate of 2.62 ± 0.17 Ga, younger than six of the other eight *Hiesinger et al*. [2000] units that comprise the *Schaber* [1973] flows.

These comparisons demonstrate that in the absence of topographically definable lava flow margins, from which the relative embayment of one unit by another can be directly established, it is difficult or impossible to reconstruct the local stratigraphic relationships from CSFD alone. As most authors assume there is no error in the crater chronology, the uncertainty of age estimates is derived from errors in establishing the CSFD of a predefined area [*Neukum*, 1983; *Hiesinger et al*., 2000, 2011]. This in turn is a function of the total sample size: increasing the size of the count area and/or including craters with smaller diameters will decrease uncertainties in the age difference between two units. Both strategies have fundamental limits. First, the maximum size of a count area is limited to the physical size of the geologic unit. Second, the resolution of the data being used and the potential effect of secondaries (see *Hiesinger et al*. [2011] for a debate on the influence of secondaries on age estimates) place a minimum on the smallest diameter craters that can be counted. Finally, despite the lunar production function remaining fixed, the impact flux has varied with time as demonstrated by the lunar chronologies [*Neukum*, 1983; *Neukum et al*., 2001; *Neukum and Ivanov*, 1994]. The corresponding rate of impact events per unit time can be approximated as exponential prior to ~3 Ga and linear thereafter. Consequently, for a given count area and crater diameter range, the uncertainty between age estimates for two areas will be lower for surfaces older than 3 Ga than for surfaces that are younger.

For example, using the error analysis applied in the popular CraterstatsII software (methodology outlined within *Michael and Neukum* [2010]) and applying the *Ivanov et al*. [2001] lunar production function and the lunar chronology of *Neukum et al*. [2001], counts conducted down to a diameter of 400 m would require count areas $>16{,}700\ \mathrm{km}^2$ (in order to accumulate a sufficient number of craters) to differentiate a surface of 2.1 Ga from one of 2.2 Ga. This criterion would only be $\sim 4600\ \mathrm{km}^2$ to differentiate two surfaces that were 3.1 and 3.2 Ga. If we follow the same calculation for crater counts down to $D = 200$ m, those surface areas would only need to be $2040\ \mathrm{km}^2$ and $560\ \mathrm{km}^2$, respectively.

The above values were derived by establishing the minimum surface area at which the error bars (associated with the two ages) ceased to overlap. The length of the bars represent a one sigma error on $N(1)$ relating to the number of craters (of a given size bin) associated with a given area for each age chosen. Please note, for simplicity, we have not incorporated the effects crater degradation—which would increase the uncertainty of the age estimates, especially for the smallest diameter craters on surfaces > 3 Ga—within our estimates. Despite the 1.5 Gyr duration of Imbrium volcanic activity, the majority of the units identified by *Hiesinger et al*. [2000] exhibit surface ages corresponding to the later third of this time span, making it difficult to differentiate between the associated CSFD in a meaningful way (given the limited size of the count areas). Regardless of the larger spread of ages within the nine units younger than 3 Ga, the linear nature of crater production since this time leads to wider error bars for these units.

To demonstrate the effect of including smaller crater diameters from high-resolution data sets, *Morota et al*. [2011] were able to refine the age estimates of some of the *Hiesinger et al*. [2000] units that correlate with the

Schaber [1973] mapped flows (Table 1) using high-resolution (10 m) Kaguya Terrain Camera data. A revised age estimate was conducted for four of the seven *Schaber* [1973] equivalent units, all of which were found to have occurred over a much shorter time span, ~2.1–2.5 Ga, than the *Hiesinger et al*. [2000] results. *Morota et al*. [2011] also showed that the embayed western unit I28 was within this age range. Although the *Morota et al*. [2011] work is more consistent with the *Schaber* [1973] results, it still fails to fully agree with the stratigraphic relationships, demonstrating that even the inclusion of smaller-diameter craters cannot resolve these issues.

An alternative strategy is thus required to refine our understanding of Imbrium volcanic stratigraphy. The mineralogical content of mare basalts is not a stochastic process but instead represents the evolution of the source magma through time. Establishing stratigraphic relationships between mare surfaces that have contrasting mineralogical properties therefore offers an alternative means to investigate the volcanic history of the lunar surface. Spectral data sets can of course identify mineralogical assemblages, and indeed, this methodology is used to constrain crater count areas as discussed above. However, the effectiveness of the corresponding mapping is modulated by the sensitivity of the method to variations in mineralogy. As discussed in section 1, spectral data sets are potentially more strongly affected by contamination from ejected material. Mare Imbrium contains multiple young large craters and rays originating from the Copernicus impact event, which cover the southern half of the basin (Figure 1a). Such ejecta deposits reduce the ability to trace boundaries between units. In contrast, radar backscatter from the lunar regolith is a combination of echoes derived from surface, volume (rock fragments suspended within the finer grain component of the regolith), and substrate scattering (the fragmented surface of the uppermost mare flow bedrock) and thus provides important information beyond the skin depth of optical instruments. The following sections demonstrate how the sensitivity of long-wavelength imaging radar data to subtle variations in TiO_2 content, and its ability to probe meters into the regolith, offers a powerful and complementary tool for mapping mare lava units.

4. Data Sets

We collected 70 cm wavelength (430 MHz frequency) synthetic aperture radar images of Mare Imbrium with a spatial resolution of 200 m/pixel following the same strategy as *Campbell et al*. [2007, 2014]. The data were obtained by transmitting a circular-polarized signal from the Arecibo Observatory and receiving the echoes from the Moon at the Green Bank Telescope (Figure 4a). This bistatic radar approach enables both senses of circular polarization to be received. Radar returns in the same sense of circular polarization (SC) as that transmitted are attributed to diffuse scattering by rocks $>$10 cm in diameter, at the surface and buried within the probing depth of the radar signal. In locations where the radar signal can penetrate the full thickness of the regolith, a component of the SC return will originate from the rocky transitional zone immediately above the bedrock [*Campbell et al*., 2014]. This unique property of the radar data provides important spatial information regarding volcanic structures, physical properties, and flow boundaries. The data sets were produced from the summation of five looks, and the resulting radar images were georectified and imported into Environmental Systems Research Institute ArcMap geographical information system database. Additional orbital remote sensing data sets were integrated, including Lunar Reconnaissance Orbiter Camera wide-angle camera (LROC WAC) 100 m resolution images and associated stereo pair-derived digital elevation models [*Scholten et al*., 2012] and Lunar Orbiter Laser Altimeter elevation data. To permit a full comparison to the *Campbell et al*. [2014] radar study of Mare Serenitatis, we also incorporated Earth-based S band (12.6 cm wavelength) data into the investigation (Figure 4b).

5. Interpreting the Spatial Patterns of Radar Backscatter From Mare Imbrium

The P band coverage of Imbrium reveals a complex distribution of radar backscatter signatures that define units of relatively uniform brightness and exhibits an ~ 18 dB range between the surface of the brightest units and the darkest (Figure 4a). The scales of these units range from tens to hundreds of kilometers in length and are distributed throughout the mare. Distinct boundaries, which display lobate and digitate forms, are traceable between some of these radar features (Figure 4a), permitting individual units to be mapped (Figure 6). The radar returns are also influenced by the ejecta blankets of young craters, tens of kilometers in diameter (Figure. 4). This effect is typically observed within one crater radius of the rim and is due to the transition

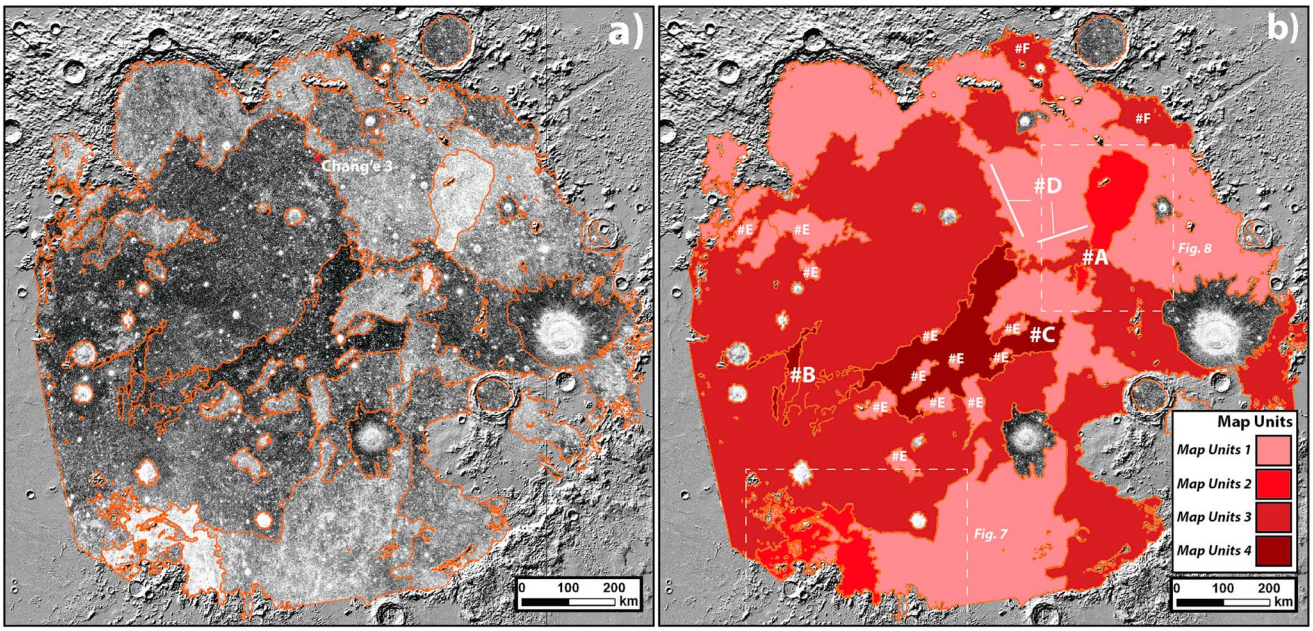

Figure 6. Radar-based map of Mare Imbrium. (a) Individual surface units overlain above the P band radar data. (b) The same map as shown in Figure 6a except with surface units shaded to correspond to the map unit with which they belong. The letters highlight features discussed in the text.

between high-density blocky material close to the crater rim and fine ejecta further out. Scattering from boulders, both surficial and interspersed within the regolith, causes a strong, central SC return surrounded by a radar dark halo due to a distal component of powdery ejecta [*Ghent et al*., 2005].

Excluding the ejecta blankets of the youngest large craters, 38 individual surface units were identified within the P band data (Figure 6a). Based on the range of radar backscatter and the relative position of the 38 units, it is possible to group them into four discrete map units (Figure 6b) in a similar manner as one would approach planetary geological mapping. This marks a contrast to previous Imbrium mapping efforts based on UV-IR data that have not attempted to group individual units [*Hiesinger et al*., 2000; *Thiessen et al*., 2014]. From this point on in the text, in order to avoid confusion, we will refer to the four groups of units (that share similar ranges in radar backscatter) as "map units" and the 38 individual units that comprise the groups as "surface units" (compare Figures 6a and 6b).

The spatial distribution of radar brightness across Imbrium broadly correlates with that of the *Lucey et al*. [2000] TiO_2 concentration map (Figure 5) derived from Clementine spectral data. The boundaries of map units 3 and 4 largely correspond with areas of Mare Imbrium with a TiO_2 content of $>3\%$. These map units display the lowest radar backscatter, a result that is expected due to the high microwave loss associated with basaltic regolith that has elevated concentrations of ilmenite. This further supports the *Campbell et al*. [2014] model of P band mare probing, in which TiO_2 induced radar loss restricts the depth of penetration into the regolith, in turn reducing the backscatter component from the rugged layer above the upper most mare flow. However, as established by *Campbell et al*. [2014], there is not always a strong correlation between the radar and the *Lucey et al*. [2000] data set, suggesting the radar is more sensitive to variations in TiO_2 content. For example, map unit 4 is delineated due to the near total absence of radar return (Figure 4a), where the *Lucey et al*. [2000] method suggests that map unit 3, not 4, contains the highest TiO_2 abundance (~10%) in Mare Imbrium.

Distinct contrasts also exist between the P band data set and orbital camera images (Figure 1a). As was previously established with Earth-based P band radar data at significantly lower spatial resolutions (tens of kilometers per pixel) [*Schaber et al*., 1970, 1975], low albedo regions within northwestern Mare Imbrium do correlate with the boundaries of the darkest radar map units (3 and 4) in this portion of the basin, but this is the extent of the similarities between the two data sets. Albedo differences across the remainder of the mare are largely dominated by ejecta material. This is especially evident in southern Imbrium, where the

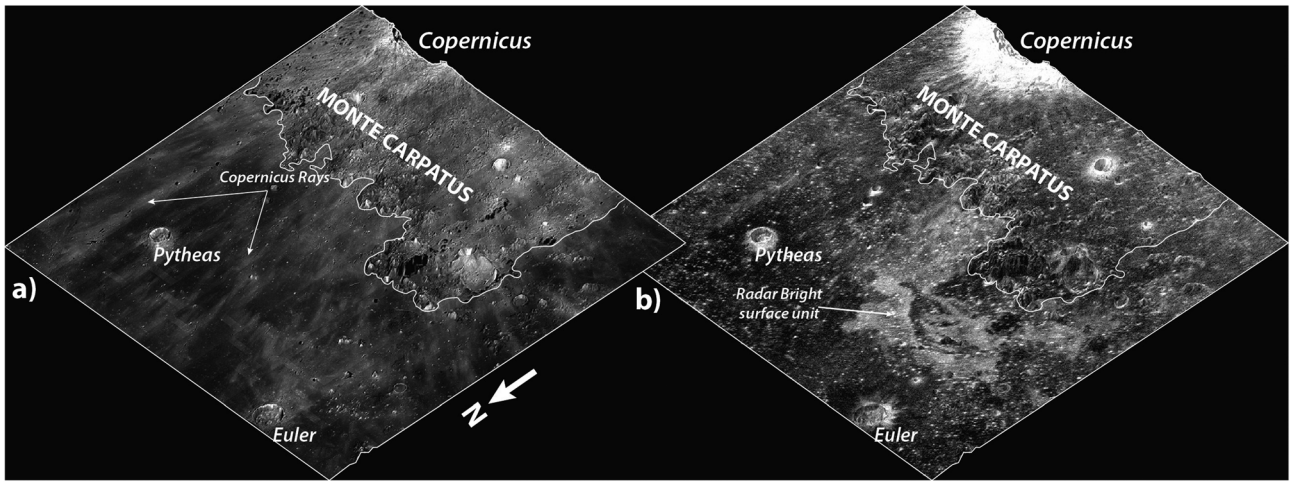

Figure 7. Perspective view comparing (a) LROC WAC mosaic with (b) P band SC radar image centered on a radar bright surface unit that belongs to map unit 2. Note that the Copernicus rays do not influence the radar image. Both data sets are draped over LROC WAC DTM. The white line in each image corresponds to the mare/highland boundary.

presence of Copernicus rays and distal ejecta hampers studies in both visible (Figure 2a) and UV-NIR spectroscopic data due to contamination of the mare surface by highland material. The ability of the P band signals to probe beneath the thin Copernicus rays permits unobstructed mapping of this quadrant. A lobate feature of enhanced radar backscatter occurs north of Monte Carpatus (Figures 4, 6, and 7). This feature represents the strongest 70 cm echoes from any nonimpact landform within Mare Imbrium. In contrast, the visible and spectrally derived maps do not delineate this feature (Figure 3).

The scale and morphology of the radar-defined units are very similar to those documented within neighboring Mare Serenitatis by *Campbell et al*., [2014], and consequently, the units are comparable to Venus and Mars lava flow fields seen in Magellan and Earth-based radar data, respectively. Based on these similarities and the broad correlations with the *Lucey et al*. [2000]-derived TiO_2 map (Figure 5), we interpret the Imbrium map units to represent the boundaries of volcanic flow fields of relatively homogeneous ilmenite content. However, unlike Mare Serenitatis, where multiple volcanic structures (such as possible collapsed lava tubes) are apparent within the radar data, similar features do not appear to be present in Mare Imbrium.

In contrast to the P band data, variations in S band radar backscatter across Mare Imbrium are significantly more modest (Figure 4b). Both data sets show corresponding regions of low backscatter within central Mare Imbrium that correlate with members of map unit 4 (Figures 4 and 6). However, in a similar manner to the visible data sets, only a few unit boundaries can be identified with the S band data, and the major variations in backscatter are derived from impact craters and associated ejecta material, including rays from Copernicus (Figure 1a). The influence of Copernicus ejecta is particularly evident along the Montes Carpatus, where the radar bright surface unit belonging to map unit 2 is clearly present in the P band data set but is not observable in the S band data (Figure 4). The inability of the S band signal to penetrate the thin rays further demonstrates that it is the penetration of the P band signal to significant depths within the mare regolith that permits a distinction to be made between volcanic features [*Campbell et al*., 2014].

6. Stratigraphic Relationships

Due to the number and relatively clear boundaries of radar-defined units in Mare Imbrium, it is possible to identify embayment relationships between the four unit groups and thus provide information on their relative stratigraphy. This is illustrated where one unit intersects or completely surrounds the boundary of another (Figure 6). The radar bright surface units in northeastern Imbrium (part of map unit 2: Figures 6b and 8) provide one of the best examples of an embayment relationship. The stratigraphically higher map unit 3 has clearly bisected the southern portion of a discrete member unit of map unit 2 (see #A on Figures 6b and 8). We translate these relationships as the consequence of embayment of volcanic flows by subsequent eruptions. From

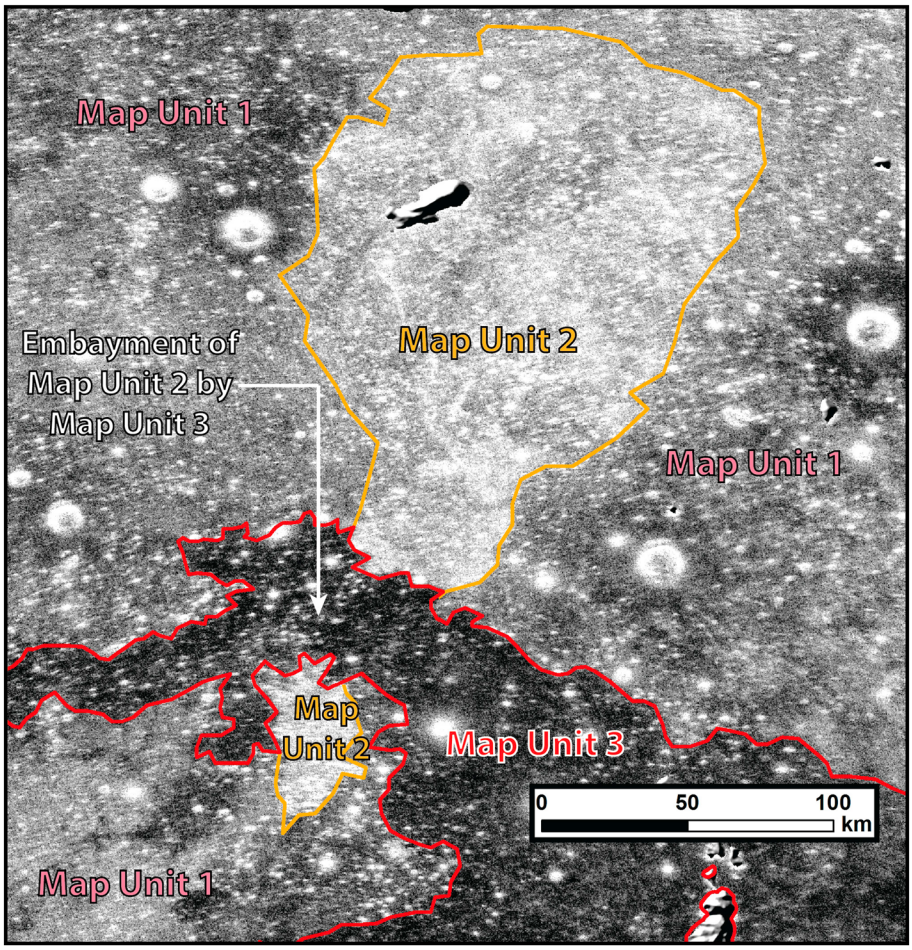

Figure 8. Portion of the P band SC radar data highlighting the stratigraphic relationships between map units 2 and 3.

this we can build up a picture of Mare Imbrium stratigraphy (Figure 9) that can be contrasted with the original stratigraphic work conducted by *Schaber* [1973] and more recent efforts [*Hiesinger et al.*, 2000; *Thiessen et al.*, 2014].

The uniqueness of Mare Imbrium, in which it contains topographically definable flows from which embayment relationships can be directly observed, provides an established stratigraphic framework [*Schaber*, 1973] for a portion of the basin in which to test the P band radar mapping. Using the low sun angle LROC wide-angle (WA) mosaic of Imbrium to emphasize subtle topographic changes, we traced all identifiable lava flow boundaries. The resulting map (Figure 2) further refines the *Schaber* [1973] work (Figure 3a). *Schaber* [1973] traced the source of the flows to a region of Mare Imbrium directly north of Euler Crater, and our flow boundary mapping finds good agreement with this. Thin, elongated (5 by 100 km) radar dark features are also present in this area and largely correlate with the topographically defined flow fronts (#B, Figure 6b). The correlation between the radar- and image-based maps demonstrates the ability of the Earth-based radar to distinguish individual small, young flows from the surrounding, older surfaces they have embayed. Based on this correspondence with the youngest of the *Schaber* [1973] mapped flows (phase III flows), we have incorporated these radar dark units, along with other units of similarly low radar backscatter, into the stratigraphically highest map unit 4.

Radar map unit 4 extends beyond the Euler source region to the northeast and terminates in the center of the basin, incorporating all of the *Schaber* [1973] flow units (phase III and II flows, see Figure 3a). However, the eastern bifurcation of radar map unit 4 (#C, Figure 6b) also incorporates a section of the stratigraphically older phase I/II flows mapped by *Schaber* [1973] based on albedo differences alone. Our new analysis of topographic flow boundaries based on the low sun angle LROC data (Figure 2) reveals that flow margins are also present along the eastern bifurcation of radar unit 4, justifying its inclusion as part of the stratigraphically youngest unit.

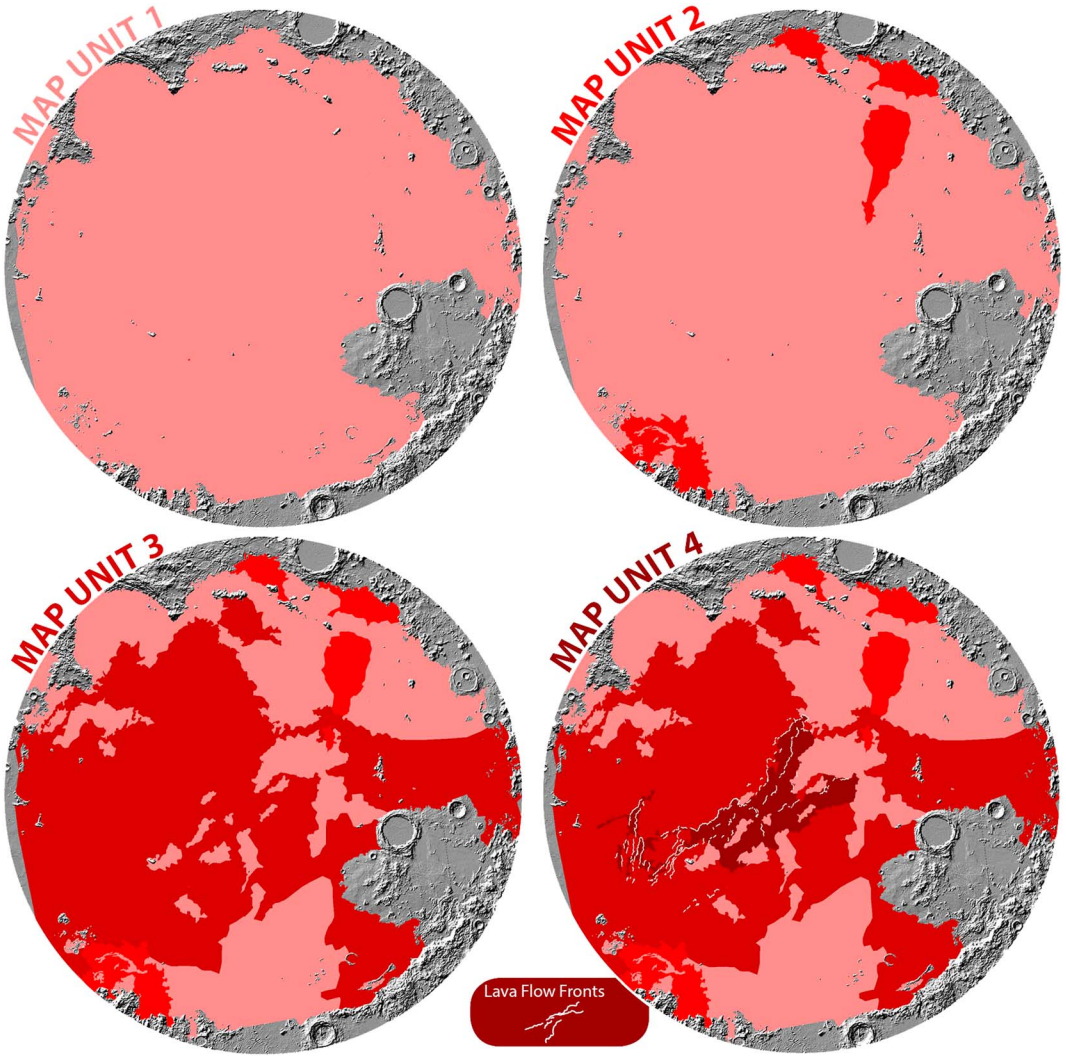

Figure 9. Interpretation of the stratigraphic relationships between the radar map units, showing the development of the current mare surface.

Tracking albedo differences across Mare Imbrium, *Schaber* [1973] mapped stratigraphically older (phase I) flows that branch out to the east and west from beyond the northern terminus of the phase II flows (Figure 3a). The northern boundary of the phase I flows are closely aligned with the boundaries of our map unit group 3 (#D, Figure 6b), though the associated radar signature extends significantly further south to cover >50% of Mare Imbrium (Figure 5). Underestimations in surface area are not the only differences between the radar and *Schaber* [1973] albedo mapping. The configuration of both radar map units 3 and 4 appears more complex relative to the *Schaber* [1973] flows. The two radar map units display examples of bifurcation, revealing exposures of older, higher radar backscatter terrain belonging to map unit 1 (#E, Figure 6b). Two isolated patches of map unit group 3 are also present along the northern boundary of Mare Imbrium (#F Figure 6b). The discrepancies between the radar data and *Schaber's* [1973] map demonstrate the limitations of albedo mapping discussed in sections 1 and 5. The units attributed to map units 1 and 2 and their relationships with map units 3 and 4 also offer information on the formation of older, pre-Eratosthenian regions of Mare Imbrium. The embayment of part of map unit 2 by map unit 3 (#A, Figures 6b and 8) and the occurrence of multiple exposures of the stratigraphically oldest unit 1, surrounded by map units 3 and 4 (#E, Figure 6b), complete the stratigraphic sequence for Mare Imbrium (Figure 7).

Taking a different approach to characterize the history of Mare Imbrium, *Fassett and Thomson* [2014] modeled the variation in surface age by mapping the level of degradation expressed by the crater population.

Unlike age dating based on CSFD, which first require count areas to be established, *Fassett and Thomson* [2014] searched for evidence of clustering exhibited by craters displaying various degrees of maturity. The resulting map displayed a concentration of pristine craters (<1.5 Ga) relative to older, degraded craters situated along the western half of Mare Imbrium that correlate with radar map unit groups 3 and 4 (Figure 6b), supporting our assessment that these are the youngest map units in Mare Imbrium. The resolution of the *Fassett and Thomson* [2014] map, like CSFD age estimates, is spatially limited relative to the rate of production of new craters over a given area. As a result, the *Fassett and Thomson* [2014] work has a spatial scale of tens of kilometers, making it impossible to discern the relationship between units smaller than the east-west divide presented in their map. The fine-scale detail revealed by the radar data in differentiating unit boundaries therefore provides an important additional tool to establish stratigraphic relationships beyond the work conducted by *Schaber* [1973].

7. Discussion

The diversity of radar-defined surface units within Mare Imbrium is greater than exhibited by Mare Serenitatis [*Campbell et al*., 2014], though this result is expected given the more extensive range in TiO_2 [*Lucey et al*., 2000; *Prettyman et al*., 2006]. As a result, Mare Imbrium can be subdivided into many more map units relative to Mare Serenitatis, permitting the development of a stratigraphic framework. Interestingly, despite the complexity of the radar returns from Mare Imbrium, fine-scale volcanic structures, such as lineal features interpreted to be collapsed lava tubes within Mare Serenitatis [*Campbell et al*., 2014], are not evident.

The distinct patterns of radar backscatter present within Mare Imbrium provide a means to geographically investigate the latter stages of volcanic activity responsible for filling the basin with over 1 km of volcanic materials. Our study provides further support for the stratigraphic relationships initially developed by *Schaber* [1973] but also yields important information regarding earlier, pre-Eratosthenian phases of volcanism. Below, we first discuss the volcanic implications of the stratigraphic relationships identified with the radar data and then we explore how our results can aid the interpretation of the Chang'e 3 LPR data.

7.1. Volcanic Implications of the Radar Stratigraphy

The stratigraphically oldest surfaces are attributed to map unit 1 (Figure 9a). Due to embayment by the three proceeding map units, it is not possible to identify any common source region(s). However, as this map unit is identifiable throughout Imbrium, it likely once covered the entire surface of the basin prior to the formation of the later map units. In comparison to map unit 1, map unit 2 is significantly limited in spatial extent, with only two discrete concentrations either adjoining or close to the main ring belt of Mare Imbrium to the north and south (Figure 9b). It is worth noting that map units 3 and 4 may have buried other occurrences of this map unit type. The isolated nature of the two surface units that comprise the map unit argues for multiple, independent source vents, and the location of the surface units may divulge regions in which individual dyke systems supplied magma to the surface. The association of the surface units with the outer region of Mare Imbrium argues that basin-wide structural control was responsible for dyke propagation, possibly as a result of extensional stresses generated by the load of the preexisting mare deposits in central Imbrium. Distinct flow units have also been identified close to the northern rim of Mare Serenitatis [*Campbell et al*., 2014].

As described above, the high TiO_2 content map units 3 and 4 are equivalent to *Schaber's* [1973] phase I, II, and III flows, though the radar data reveals the older map group 3 to extend over a much greater area of Mare Imbrium than mapped from albedo changes alone (Figure 2a). The radar properties are largely homogeneous over much of western Imbrium, and consequently, this whole area has been mapped as part of map unit 3. Clementine [*Hiesinger et al*., 2000] and M^3 [*Thiessen et al*., 2014] studies have both subdivided this western region into multiple, spatially correlated units.

The P band data reveals a braided pattern in which isolated regions of map unit 1 are completely enclosed by map unit 3 in western Imbrium and by both map unit 3 and 4 in central Imbrium (#E, Figures 6b, 7c, and 7d). We argue that these smaller units represent kipukas formed by the emplacement of the high TiO_2 flows within an extensive region of earlier, lower TiO_2 flows. The occurrence of kipukas is significant in that despite the extensive spatial coverage of map unit 3, the associated lava flows must have been relatively thin in order not to have completely embayed the preexisting TiO_2 surfaces. This is also the case for map unit 4, which appears to have flowed over the central portion of map unit 3, also leaving kipukas of the older mare surface.

Schaber [1973] argued that the source region of the high TiO_2 flows was a now-buried section of Mare Imbrium close to Euler crater. This interpretation is consistent with P band data in that we observe thin, elongated (~10 km) regions of low radar backscatter (several of which are located within the margins of topographically distinct flows (see Figure 7d) which originate north of Euler). In agreement with *Schaber* [1973], we argue these radar signatures represent the final individual lava flows erupted in Mare Imbrium.

The occurrence of numerous kipukas throughout Mare Imbrium offers an advantageous sampling strategy to future rover missions. Throughout central and western Imbrium, multiple surfaces exhibiting distinct ages and chemistry can be easily accessed over relatively short transverses. For example, a rover landing close to #C in Figure 6b would be able to visit portions of map units 1, 3, and 4. As unit 4 includes some of the youngest flows recognized on the Moon [*Schaber*, 1973], such a landing site would potentially permit a rover to sample an extensive age range of mare volcanism.

7.2. Chang'e 3 Landing Site

The P band map (Figure 6) provides additional context in which to interpret the landing site of the Chinese Chang'e 3 lander and rover. Preexisting mapping of Mare Imbrium, based on spectral and albedo data, established that Chang'e 3 landed close to a distinct boundary in mare TiO_2 content in the northwestern branch of *Schaber's* [1973] flow unit I (Figure 3a). The P band data corroborates this interpretation, as the landing site is clearly located within the relatively dark (hence high TiO_2) map unit 3, 4 km to the south of a boundary with map unit 1. In contrast the S band data set provides little regional context as no broad distinctions can be identified in backscatter across western Imbrium. However, due to the high spatial resolution of the S band data, the 450 m crater close to the Chang'e-3 landing site is resolvable.

Our interpretation of the radar-based stratigraphy of the Chang'e 3 landing site is more in line with *Xiao et al*. [2015], rather than the *Zhang et al*. [2015] evaluation of results from the LPR. *Xiao et al*. [2015] suggest the uppermost stack of Eratosthenian mare flows (labeled vertical unit "d," within their publication) is thin ($<$50 m thick) and is vertically separated from lower flows by impact regolith, suggesting a long hiatus between the two sets of volcanic flows. Our analysis agrees with this in that we argue (1) radar map unit 3 is relatively thin (despite being areally extensive) and (2) at the Chang'e 3 landing site, map unit 3 overlies the stratigraphically oldest map unit 1, suggesting there was a significant interval between periods of volcanic activity. We therefore suggest the putative lower, older flows inferred from the LPR data by *Xiao et al*. [2015] (and referred to as vertical unit "f," within their publication) belong to map unit 1. If the northern terminus of map unit 3 flows were thick (~200 m), as suggested by *Zhang et al*. [2015], it is difficult to reconcile how kipukas of map unit 1 would not have been fully embayed.

8. Conclusion

We have presented a new view of the volcanic stratigraphy of Mare Imbrium using high-resolution P band Earth-based radar data. As was established in Mare Serenitatus by *Campbell et al*. [2014], the penetration of the P band signal is strongly influenced by small variations in the TiO_2 content of the lunar regolith resulting in significant shifts in radar backscatter. Consequently, due to the relatively large range in TiO_2 content of the Mare Imbrium basalts, the radar data reveals a diverse pattern of radar backscatter, including the existence of distinct boundaries between regions of differing radar brightness. Tracing these boundaries enabled us to identify 38 individual units, which based on radar brightness can be subdivided into four "map" units.

Mare Imbrium is quite unique in that topographically definable Eratosthenian-aged lava flows are present within the southwest-center of the basin. Previous mapping of these flows has established a stratigraphic framework [*Schaber*, 1973], which serves as a means to test the radar-based work. We find a strong spatial agreement between the two mapping approaches, which gives us confidence to extend our stratigraphic framework beyond the southwest-central region of Mare Imbrium to incorporate the whole basin. Through our mapping, we conclude the following

1. Thin, elongated (~10 km wide) regions of low radar backscatter (several of which are located within the margins of topographically distinct flows) are situated downslope of Euler crater. This supports *Schaber* [1973] assertion that the Eratosthenian flows originated from a now-buried vent close to Euler.

2. The presence of kipukas within the high TiO_2 map units 3 and 4 suggest that although the later phases of activity in Mare Imbrium resulted in spatially extensive flow units, the associated lava flows must have been relatively thin in order not to have completely embayed the preexisting low TiO_2 surfaces.
3. The radar mapping suggests that pre-Eratosthenian, low TiO_2 volcanic emplacement originated from several source regions within the Imbrium basin, including the mare surface north of Monte Carpatus. The radar proved particularly valuable in delineating units within this region because the presence of extensive Copernicus ejecta material prevents effective mapping using visible and UV-NIR spectral data sets.
4. Finally, the radar map places important constraints on the interpretation of the Chang'e-3 lunar penetrating radar measurements and reveals the locations of regions where a range of mare volcanism could be sampled over small areas by a future lander/rover.

Acknowledgments

This paper reflects many years of B.R. Hawke's advice to the authors on a diverse range of lunar science topics. His deep knowledge of the Moon and wise counsel will be greatly missed. We would like to thank B. Thomson, an anonymous reviewer, and JGR Associate Editor W. Fa for their detailed feedback and helpful suggestions. This work was supported in part by grants from NASA's Planetary Astronomy and LASER Programs. The SC radar image data used to derive the Mare Imbrium map are available in tiff format on the Center for Earth and Planetary Studies at the National Air and Space Museum website and can be found at http://airandspace.si.edu/CEPSData. The authors thank the staff at Arecibo Observatory and the Green Bank Telescope for invaluable assistance in collecting the lunar radar data. John Chandler of the Smithsonian Astrophysical Observatory provided the lunar ephemerides for our mapping. The Arecibo Observatory is operated by SRI International under a cooperative agreement with the National Science Foundation (AST-1100968) and in alliance with Ana G. Méndez-Universidad Metropolitana and the Universities Space Research Association. The Arecibo Planetary Radar Program is supported by the National Aeronautics and Space Administration under grant NNX12AF24G issued through the Near Earth Object Observations Program. The Green Bank Telescope is part of the National Radio Astronomy Observatory, a facility of the NSF operated under cooperative agreement by Associated Universities, Inc.

References

Borg, L. E., A. Gaffney, and D. DePaolo (2007), Rb–Sr and Sm–Nd isotopic systematics of NWA032. *Proc. 70th Annual Meteorit. Soc. Meeting*, Abstract 5232.

Braden, S. E., J. D. Stopar, M. S. Robinson, S. J. Lawrence, C. H. van der Bogert, and H. Hiesinger (2014), Evidence for basaltic volcanism on the Moon within the past 100 million years, *Nat. Geosci.*, *7*(11), 787–791.

Bryan, S. E., and L. Ferrari (2013), Large igneous provinces and silicic large igneous provinces: Progress in our understanding over the last 25 years, *Geol. Soc. Am. Bull.*, *25*, doi:10.1130/B30820.1.

Bugiolacchi, R., and J. Guest (2008), Compositional and temporal investigation of exposed lunar basalts in the Mare Imbrium region, *Icarus*, *197*(1), 1–18, doi:10.1016/j.icarus.2008.04.001.

Campbell, B. A., B. R. Hawke, and T. W. Thompson (1997), Long-wavelength radar studies of the lunar maria, *J. Geophys. Res.*, *102*, 19,307–19,320, doi:10.1029/97JE00858.

Campbell, B. A., D. B. Campbell, J. L. Margot, R. R. Ghent, M. Nolan, J. Chandler, L. M. Carter, and N. J. S. Stacy (2007), Focused 70-cm radar mapping of the Moon, *IEEE Trans. Geosci. Remote Sens.*, *45*(12), 4032–4042, doi:10.1109/TGRS.2007.906582.

Campbell, B. A., L. M. Carter, B. R. Hawke, D. B. Campbell, and R. R. Ghent (2008), Volcanic and impact deposits of the Moon's Aristarchus Plateau: A new view from Earth-based radar images, *Geology*, *36*, 135–138, doi:10.1130/G24310A.1.

Campbell, B. A., B. R. Hawke, L. M. Carter, R. R. Ghent, and D. B. Campbell (2009), Rugged lava flows on the Moon revealed by Earth-based radar, *Geophys. Res. Lett.*, *36*, L22201, doi:10.1029/2009GL041087.

Campbell, B. A., L. M. Carter, D. B. Campbell, M. Nolan, J. Chandler, R. R. Ghent, B. R. Hawke, R. F. Anderson, and K. Wells (2010), Earth-based S-band radar mapping of the Moon: New views of impact melt distribution and mare physical properties, *Icarus*, doi:10.1016/j.icarus.2010.03.011.

Campbell, B. A., B. Ray Hawke, G. A. Morgan, L. M. Carter, D. B. Campbell, and M. Nolan (2014), Improved discrimination of volcanic complexes, tectonic features, and regolith properties in Mare Serenitatis from Earth-based radar mapping, *J. Geophys. Res. Planets*, *119*, 313–330, doi:10.1002/2013JE004486.

De Hon, R. A. (1979), Thickness of the western mare basalts, *Proc. Lunar Planet. Sci. Conf.*, 10th, 2935–2955.

Fa, W., M. H. Zhu, T. Liu, and J. B. Plescia (2015), Regolith stratigraphy at the Chang'E-3 landing site as seen by lunar penetrating radar, *Geophys. Res. Lett.*, *42*, 10,179–10,187, doi:10.1002/2015GL066537.

Fassett, C. I., and B. J. Thomson (2014), Crater degradation on the lunar maria: Topographic diffusion and the rate of erosion on the Moon, *J. Geophys. Res. Planets*, *119*, 2255–2271, doi:10.1002/2014JE004698.

Ghent, R. R., D. W. Leverington, B. A. Campbell, B. R. Hawke, and D. B. Campbell (2005), Earth-based observations of radar-dark crater haloes on the Moon: Implications for regolith properties, *J. Geophys. Res.*, *110*, E02005, doi:10.1029/2004JE002366.

Head, J. W. (1975), Lunar mare deposits: Areas, volumes, sequence, and application for melting in source areas, in *Conference on Origins of Mare Basalts and Their Implications for Lunar Evolution*, pp. 66–71, Lunar Science Institute, Houston, Tex.

Head, J. W. (1982), Lava flooding of ancient planetary crusts: Geometry, thickness, and volumes of flooded lunar impact basins, *Moon Planets*, *26*(1), 61–88, doi:10.1007/BF00941369.

Head, J. W., and M. F. Coffin (1997), Large igneous provinces: A planetary perspective, in *Large Igneous Provinces: Continental, Oceanic, and Planetary Flood Volcanism*, *Geophys. Monogr. Ser.*, vol. 100, edited by J. Mahoney and M. Coffin, p. 411–438, AGU, Washington, D. C., doi:10.1029/GM100p0411.

Hiesinger, H., R. Jaumann, G. Neukum, and J. W. Head (2000), Ages of mare basalts on the lunar near side, *J. Geophys. Res.*, *105*, 29,239–29,275, doi:10.1029/2000JE001244.

Hiesinger, H., J. W. Head III, U. Wolf, R. Jaumann, and G. Neukum (2003), Ages and stratigraphy of mare basalts in Oceanus Procellarum, Mare Nubium, Mare Cognitum, and Mare Insularum, *J. Geophys. Res.*, *108*(E7), 5065, doi:10.1029/2002JE001985.

Hiesinger, H., J. Head, U. Wolf, R. Jaumann, and G. Neukum (2011), Ages and stratigraphy of lunar mare basalts: A synthesis, in *Recent Advances and Current Research Issues in Lunar Stratigraphy*, edited by W. A. Ambrose and D. A. Williams, *Geol. Soc. Am. Spec. Pap.*, *477*, 1–51.

Ivanov, B. A., G. Neukum, and R. Wagner (2001), Size-frequency distributions of planetary impact craters and asteroids, in *Collisional Processes in the Solar System*, edited by M. Y. Morov and H. Rickmann, pp. 1–34, Kluwer Acad., Norwell, Mass.

Lucey, P. G., D. T. Blewett, and B. D. Jolliff (2000), Lunar iron and titanium abundance algorithms based on final processing of Clementine UV-Visible images, *J. Geophys. Res.*, *105*, 20,297–20,306, doi:10.1029/1999JE001117.

Michael, G. G., and G. Neukum (2010), Planetary surface dating from crater size-frequency distribution measurements: Partial resurfacing events and statistical age uncertainty, *Earth Planet. Sci. Lett.*, *294*(3-4), 223–229, doi:10.1016/j.epsl.2009.12.041.

Morota, T., et al. (2011), Timing and characteristics of the latest mare eruption on the Moon, *Earth Planet. Sci. Lett.*, *302*(3-4), 255–266, doi:10.1016/j.epsl.2010.12.028.

Neukum, G. (1983), Meteoritenbombardement und Datierung Planetarer Oberflächen, Habilitationsschrift, Univ. of München, Munich, Germany.

Neukum, G., and B. A. Ivanov (1994), Crater size distribution and impact probabilities on Earth from lunar, terrestrial-planet, and asteroid cratering data, in *Hazards Due to Comets and Asteroids*, edited by T. Gehrels, pp. 359–416, Univ. of Arizona, Tucson.

Neukum, G., B. A. Ivanov, and W. K. Hartmann (2001), Cratering records in the inner solar system in relation to the lunar reference system, *Space Sci. Rev.*, *96*, 55–86.

Nyquist, L. E., and C.-Y. Shih (1992), The isotopic record of lunar volcanism, *Geochim. Cosmochim. Acta*, *56*, 2213–2234.
Nyquist, L. E., D. D. Bogard, and C.-Y. Shih (2001), Radiometric chronology of the Moon and Mars, in *The Century of Space Science*, edited by J. A. Bleeker, J. Geiss, and M. Huber, pp. 1325–1376, Kluwer Acad., Netherlands.
Ono, T., A. Kumamoto, H. Nakagawa, Y. Yamaguchi, S. Oshigami, A. Yamaji, T. Kobayashi, Y. Kasahara, and H. Oya (2009), Lunar radar sounder observations of subsurface layers under the nearside maria of the Moon, *Science*, *323*(5916), 909–912.
Peeples, W. J., W. R. Sill, T. W. May, S. H. Ward, R. J. Phillips, R. L. Jordan, E. A. Abbott, and T. J. Killpack (1978), Orbital radar evidence for lunar subsurface layering in Maria Serenitatis and Crisium, *J. Geophys. Res.*, *83*, 3459–3468, doi:10.1029/JB083iB07p03459.
Pieters, C. M. (1978), Mare basalt types on the front side of the moon: A summary of spectral reflectance data, *Proc. Lunar Planet. Sci. Conf.*, 9th, 2825–2849.
Prettyman, T. H., J. J. Hagerty, R. C. Elphic, W. C. Feldman, D. J. Lawrence, G. W. McKinney, and D. T. Vaniman (2006), Elemental composition of the lunar surface: Analysis of gamma ray spectroscopy data from Lunar Prospector, *J. Geophys. Res.*, *111*, E12007, doi:10.1029/2005JE002656.
Schaber, G. G. (1973), Lava flows in Mare Imbrium: Geologic evaluation from Apollo orbital photography, *Proc. Lunar. Planet. Sci. Conf.*, *4*(1), 73–92.
Schaber, G. G., R. E. Eggleton, and T. W. Thompson (1970), Lunar radar mapping: Correlation between radar reflectivity and stratigraphy in north-western Mare Imbrium, *Nature*, *226*, 1236–1239.
Schaber, G. G., T. W. Thompson, and S. H. Zisk (1975), Lava flows in Mare Imbrium: An evaluation of anomalously low earth-based radar reflectivity, *The Moon*, *13*(4), 395–423.
Scholten, F., J. Oberst, K.-D. Matz, T. Roatsch, M. Wählisch, E. J. Speyerer, and M. S. Robinson (2012), GLD100: The near-global lunar 100 m raster DTM from LROC WAC stereo image data, *J. Geophys. Res.*, *117*, E00H17, doi:10.1029/2011JE003926.
Soderblom, L. A., J. A. Arnold, J. M. Boyce, and R. P. Lin (1977), Regional variations in the lunar maria: Age, remanent magnetism, and chemistry, *Proc. Lunar Sci. Conf.*, 8th, 1191–1199.
Taylor, L. A., J. Shervais, R. Hunter, C. Y. Shih, B. M. Bansal, J. Wooden, L. E. Nyquist, and J. C. Laul (1983), Pre-4.2 AE mare basalt volcanism in the lunar highlands, *Earth Planet. Sci. Lett.*, *66*, 33–47, doi:10.1016/0012-821X(83)90124-3.
Taylor, S. R. (1982), *Planetary Science: A Lunar Perspective*, Lunar and Planetary Institute, Houston, Tex.
Thiessen, F., S. Besse, M. I. Staid, and H. Hiesinger (2014), Mapping lunar mare basalt units in mare Imbrium as observed with the Moon Mineralogy Mapper (M^3), *Planet. Space Sci.*, *104*, 244–252, doi:10.1016/j.pss.2014.10.003.
Thomson, B. J., E. B. Grosfils, D. B. J. Bussey, and P. D. Spudis (2009), A new technique for estimating the thickness of mare basalts in Imbrium Basin, *Geophys. Res. Lett.*, *36*, L12201, doi:10.1029/2009GL037600.
Weider, S. Z., I. A. Crawford, and K. H. Joy (2010), Individual lava flow thicknesses in Oceanus Procellarum and Mare Serenitatis from Clementine multispectral data, *Icarus*, *209*, 323–336, doi:10.1016/j.icarus.2010.05.010.
Xiao, L., et al. (2015), A young multilayered terrane of the northern Mare Imbrium revealed by Chang'E-3 mission, *Science*, *347*(6227), 1226–1229.
Zhang, J., et al. (2015), Volcanic history of the Imbrium basin: A close-up view from the lunar rover Yutu, *Proc. Natl. Acad. Sci. U.S.A.*, *112*(17), 5342–5347, doi:10.1073/pnas.1503082112.
Ziethe, R., K. Seiferlin, and H. Hiesinger (2009), Duration and extent of lunar volcanism: Comparison of 3D convection models to mare basalt ages, *Planet. Space Sci.*, *57*(7), 784–796, doi:10.1016/j.pss.2009.02.002.